ICONHIC2019
2nd International Conference on Natural Hazards & Infrastructure
23-26 June,2019, Chania, Greece

Analysis of slope instabilities in the Corinth Canal using UAV-enabled mapping

C. Saroglou[1], V. Kallimogiannis[1]
[1]*Department of Civil Engineering, National Technical University of Athens, Greece,*
saroglou@central.ntua.gr
N. Bar[2]
[2]*Gecko Geotechnics, Cairns, Australia*
G. Manousakis[4]
[4]*ElxisGroup, Geomatics Engineer, Greece*
D. Zekkos[3]
[3]*Department of Civil and Environmental Engineering, University of Michigan, USA*

ABSTRACT

The Corinth Canal crosses the Isthmus of Corinth and is of great importance for Mediterranean navigation as well as for railroad and highway connectivity between southern and central Greece. Since its operation, in 1893, the slopes have shown stability problems due to their steepness, the mechanical behavior of the Corinth Canal marl and the strong earthquakes that have frequently occurred in the region. In February and March 2018, two slope instabilities of the cut that resulted in the closure of the Canal for a few days. A high resolution survey was conducted using an unmanned aerial vehicle (UAV) with an ultrahigh definition (UHD) camera, which produced 3D point clouds and high-resolution orthophotos of the affected areas. The volumes of these two slope failures were estimated at 6000 m^3 and 700 m^3 respectively. The paper presents the UAV-based mapping and subsequent three-dimensional slope stability analysis of the recent failures, highlighting the value of such an approach for an expedited and accurate determination of the slope geometry and the features controlling the instability of the slopes. Finally, the potential risk of instability along the Canal based on the recent event is discussed.

Keywords: Corinth Canal, Unmanned aerial vehicles, Structure-from-Motion, 3D slope stability, failure

INTRODUCTION

Since the beginning of the operation of the Corinth Canal, in 1893, the slopes have experienced stability problems due to the very steep inclination, the mechanical behavior of the Corinth Canal marl and the strong earthquakes that have affected the region. The Canal is approximately 6.3 km long, 21 m wide with 8±2 m depth of water and slopes that vary in height along the cut, but may reach 75 m. The most severe instability throughout the canal's operation, occurred in November 1923, when a large failure blocked the canal entirely. Since 1940, the landslides and rockfalls have been less severe and are mainly associated with earthquakes in the area. Some of the failures are also caused due to undercutting of the slope at its base caused by wave action and associated erosion. The cut failures have wedge or prismatic shapes that are formed by the intersection of the fault surfaces encountered along the canal in combination with the main fractures that are formed by slope relaxation (Marinos et al., 2001).

Based on the slope stability analyses, which were performed in the past (Kavvadas, 1990), it was concluded that it is not likely that the slope failures occur through the marl formation in the form of circular slides, but mainly along the discontinuities.

The risk of a large failure of the Canal slopes remains high, as demonstrated by the large failure that occurred on February 26 2018 and is shown in Figure 1. The safe operation of the canal may be endangered by the occurrence of slope failures and it is thus necessary to determine the risk from slope instabilities along the entire length of the canal and identify the higher risk areas. The use of new technologies, such as UAV-enabled mapping, in combination with field reconnaissance provides a very effective method of identifying the risk areas along the canal and calculating the slope stability conditions considering different loading scenarios, such as water pressure and seismic loading.

In the present study, the slope instability of the recent slope failure is analyzed using UAV-enabled mapping and limit equilibrium three-dimensional stability analysis, in order to demonstrate the effectiveness of this methodology and back-calculate the strength of the failed rock mass. Examples of immediate UAV-enabled infrastructure reconnaissance following natural disasters in Greece are given in Zekkos et al. (2016), while a detailed review of the application of UAV-enabled structure-from-motion photogrammetry in geotechnical engineering can be found in Zekkos et al. (2018). A review of the use of remotely piloted aircraft systems (RPASs), a subcategory of UAVs, for the management of natural hazards has been also presented by Giordan et al. (2018). UAV-enabled mapping has been used recently in case studies in Greece for back analysis of a co-seismic rockfall (Saroglou et al., 2018), and a landslide following the 2015 earthquake in Lefkada (Kallimogiannis et. al. 2019).

Figure 1. View of the slope failure, which occurred on February 26 2018 at the south slope of the Corinth Canal.

GEOLOGICAL – GEOTECHNICAL CONDITIONS

Geological setting

The broader area of isthmus of Corinth belongs to the Sub-Pelagonian geotectonic zone of Greece, which includes: a) Paleozoic limestones, sandstones and basic igneous rocks, b) Mesozoic limestones, radiolarites, shales and ophiolites, c) Plio-pleistocene, lacustrine and marine alternations of marls, sandstones, conglomerates and marly limestones, d) volcanic rocks (dacites) and e) fluviatile and marine sandstones and conglomerates of Pleistocene. The geological formations along the Canal have been affected by a series of normal faults, while the blocks limited between the faults are crossed by a major system of sub-vertical joints running parallel to the faults at an angle of 30 – 40^0 with respect to the Canal axis.

Freyberg (1973), in a more detailed mapping of the Canal slopes, reported that almost 45 main faults transverse the canal, which create a series of tectonic grabens and horsts. All major faults and their relative movement can be easily observed on both sides of the Canal.

Geotechnical conditions

According to Andrikopoulou et al. (1988), along the canal starting from Poseidonia (W) to Isthmia (E), the following geotechnical zones are encountered, as shown in Figure 2:

- Zone 1: Soil-like formations consisting of Plio-Pleistocene sands, clays and silts (location 0-1200 and 5350 – 5750 m).
- Zone 2: Zone with more structural perturbances consisting of soil-like to weak rock formations, mainly sands and gravels, coarse sandstones, conglomerates, marls and marly limestones (location 1200 – 1500 m).
- Zone 3: A highly unstable zone consisting of coarse sand and gravel and marls (location 1500–2000).
- Zone 4: Zone consisting of marls and marly limestones with intercalations of sandstones and conglomerates.
- Zone 5: The area consists of sandstones, conglomerates, marls and marly limestones. It resembles to Zone 3, but the formations have higher strength due to higher degree of diagenesis.

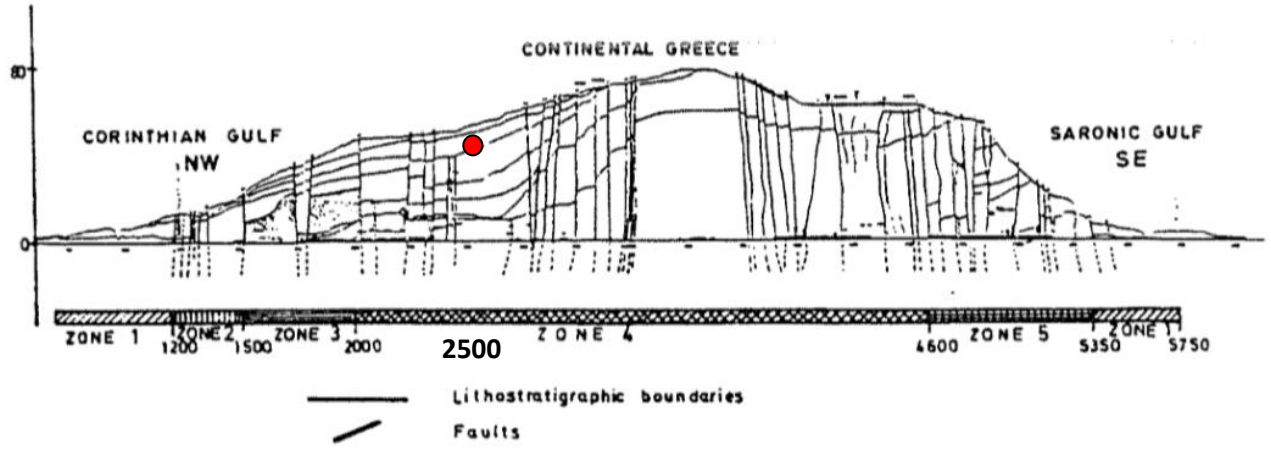

Figure 2. Geotechnical zoning of the Corinth Canal (from Andrikopoulou et al. 1988). The location of the slope failure is denoted.

UAV MAPPING

Field data acquisition consisted of two flights above the failed slopes. The first failure occurred on February 26 2018 and the field mapping was conducted on March 6th 2018. Eleven days after the first failure, on March 9th 2018 a second failure took place, and was mapped on March 16th 2018. Mapping involved the acquisition of approximately 600 oblique photos with the goal to capture the geometric details on the steep side slopes of the canal. Aerial mapping was conducted using a DJI Phantom 4 Pro quadrotor drone, equipped with an 1-inch 20 MP CMOS sensor with mechanical shutter (image size captured 3:2 Aspect Ratio: 5472 × 3648 pixels).

Oblique imagery was collected at 30 m mean height above ground level which resulted in an average ground sampling distance of 1.7 cm, featuring an 80% frontal and 70% side overlap that was adequate for the Structure-from-Motion block adjustment processing and analysis.

Structure-from-Motion (SfM) is a photogrammetric and computer vision technique that uses overlapping imagery to identify matching features in multiple images. Compared to a classic photogrammetric technique where the location of the camera is known, in SfM a non-linear least-squares minimization technique is used to iteratively estimate the 3D relative location of both camera positions and object coordinates, and a sparse bundle adjustment is implemented to transform the measured image coordinates to three dimensional points of the area of interest (Westoby et al. 2012, Zekkos et al. 2018). Subsequently, the 3D point cloud is densified beyond the identified features. For this project, no ground control points were collected, since

precise geolocation was not necessary and the results of Bundle Block Adjustment (mean reprojection error and camera's internal and external parameters) establish an accurate reproduction of the 3D geometry.
In this study, the technique was implemented using the two software packages: *Pix4D* (Pix4D S.A., Switzerland) and *ShapeMetrix UAV* (3GSM GmbH, Austria). Specifically, the following geospatial outputs were generated for each failure using *Pix4D*:

(a) 3D point clouds: The reconstruction of the surface model including most visible surface details (man-made feature elements, vegetation, etc.) is primarily achieved by a set of densified 3D points, which stores X, Y, Z coordinates information in the desired coordinate system and RGB color information for each point, derived by photo correlation while performing SfM processing.

(b) Orthophotos: Using 2.5D DSMs projected on the almost vertical planes of the slopes for removing perspective distortion from the images (orthorectification method), true orthophotos were generated by orthomosaicing overlapping aerial images. True orthophotos correct for the perspective of the camera lens and have a constant scale for the entire area mapped and therefore can be used for 2D measurements.

Figure 3. Point cloud of slope failure of Corinth Canal on February 26th and March 9th from Pix4D.

SLOPE FAILURES

Mechanism of failure

The instabilities in the Canal have usually the shapes of prisms or wedges and are formed by the intersection of fault surfaces with main discontinuities. Based on previous studies, it is evident that no circular failures have occurred through the marl formation and the only type of instability are due to relaxation and eventual formation of prisms from the Canal walls. Although the marl formations do not have a high hydrostatic water table, which favors stability, the fault planes are often water conduits and instabilities have occurred in the past during periods of heavy rainfall. The main slides of the Canal have occurred in the past in Zone 3, between location 1500 to 2000 m while some minor instability problems have occurred in Zone 4, between 2000 and 4600 m.

The 2018 failures occurred at the south slope at location 2500 m, an area belonging to Zone 4 per Andrikopoulou et al. 1988. The slope at this section has a slope angle of 80^0 and a total height of 45 m. The width of the affected zone by the first failure was approximately equal to 50 m and the height of the formed wedge was 45 m. As presented earlier, the slopes in this area are formed by marls and marly limestones with intercalations of sandstones.

The slope failure was due to the relaxation of the slope along the main joint, which intersects the fault present at that location. The failure may have been also triggered by rainfall, which occurred 3-4 days earlier. Based on the field survey, it was determined that the prism was detached along the joint which formed a tensile crack for the largest part of the slope (up to 40 m), while at the base, the failure occurred through the intact marl horizon. The slope geometry before the failure was not available and it was determined by extending the slope surface from the adjacent area to the failure. The volume of the failed block of the

February 26th event, was calculated by differencing of the pre- and post-failure slope geometry in CloudCompare (GPL, 2015) and was determined equal to 6000 m^3 (weight equal to 12000 tn). In order to analyze the kinematic stability of the wedge, it was necessary to determine the orientation of the planes controlling the failure.

Discontinuity analysis

The geometry of the faults and main discontinuity sets were determined from the 3D photogrammetric models using photos captured from the UAV and the ShapeMetriX UAV (3GSM GmbH, Austria) software. Layers of marl and marly limestone were differentiated by mapping visibly different bands or beds of strata in three-dimensions. Similarly, other geological features, such as faults, joints and failure back scarps were also digitally mapped in 3D to identify the spatial location (X, Y and Z coordinates), the orientation of the planes (dip and dip direction), and the length or surface area of the planes. The identified discontinuities are presented in Figure 3. The Schmidt projection of the discontinuities is shown in Figure 4 and their mean orientations and geometrical characteristics are presented in Table 1.

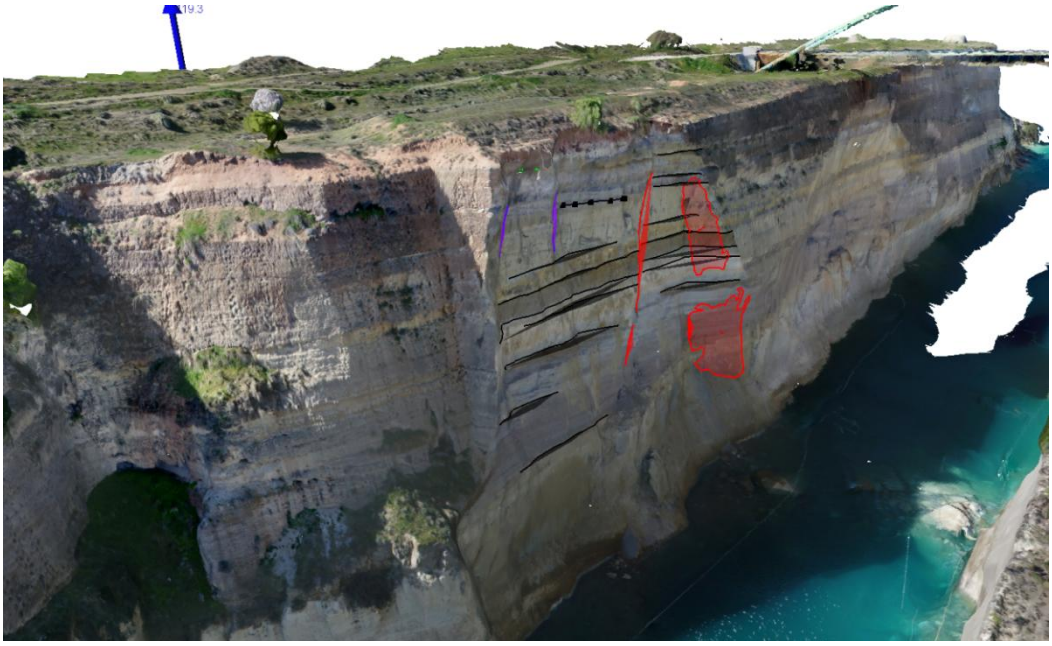

Figure 3. 3D Model from ShapeMetriX UAV illustrating faults and main discontinuity surfaces controlling the slope failure of 26th February (fault surfaces in red, joint surfaces in blue, bedding surfaces in black).

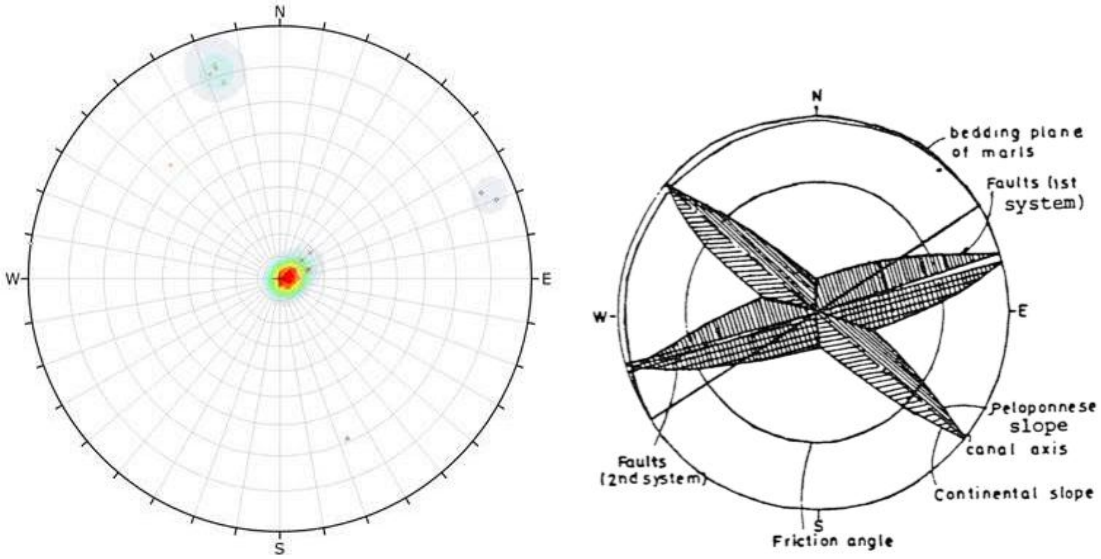

Figure 4. a) Lower hemisphere equal angle stereographic projection of main discontinuity surfaces controlling the slope failure. b) Structural data of the canal slopes (Andrikopoulou et al., 1988).

Table 1. Mean orientation and geometry of faults, bedding and discontinuity surfaces

	Dip/Dip Direction	Length (m) (min-max)	Area (m^2)
Fault	71/149	18.2 – 22.9	
Joint	80/163	5.7 – 7.2	
Backscarp	70/290	-	23.7 – 120.1
Bedding	06/272	6.7 – 32.8	

SLOPE STABILITY BACK-ANALYSIS

Planar failure stability

The failed block was a long pillar, bounded on the sides by the fault and the joint surface, rather than a wedge. Therefore, an initial stability assessment of the slope was conducted using a two dimensional limit equilibrium analysis against planar sliding using Rocplane (Rocscience Inc, 2002).
Based on the geometry of the main discontinuity forming the scarp, and considering the initial slope geometry, a back-analysis of the February 26 failure, was performed. The back-analysis was conducted considering a planar slide of a block at the base of the slope with failure through the intact marl and a tensile crack at the back scarp of the failure.
The total height of the failed block was 45 m and the distance of the tensile crack from the slope face was 3 m. The shear strength of the marl at the base of the failed block was determined equal to c'=150 kPa $\varphi=35^0$ while no strength was attributed to the back scarp tensile surface. The factor of safety was calculated equal to 1.0. Based on the planar stability analysis shown in Figure 5, and for an assumed total unit weight of 2.0 tn/m^3, the wedge weight of the block was 267 tn/m, resulting in a total weight of the failed block equal to 13350 tn. This agrees well with the weight determined by surface differencing of the pre- and post-failure slope geometry in Cloudcompare, which was 6000 m^3 (equivalent to 12000 tn).

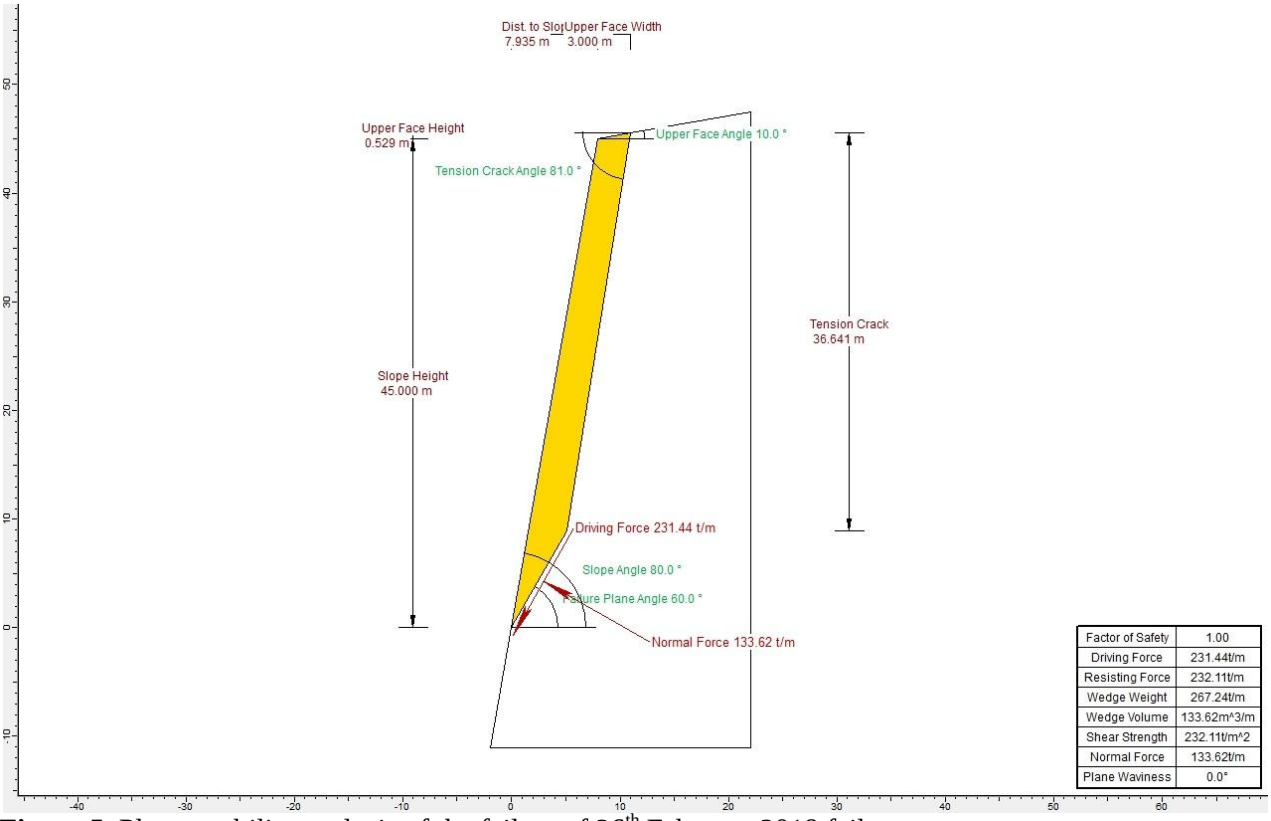

Figure 5. Planar stability analysis of the failure of 26th February 2018 failure.

3D Slope stability

In most cases, failures in rock slopes are three-dimensional in nature and have both geological structure and rock mass failure components (Bar & McQuillan, 2018). This is certainly the case for the failure of February 26 2018 as demonstrated in the planar stability analysis.

Three-dimensional limit equilibrium analysis (3D LEA) software, *Slide*^{3} *2019* (Rocscience Inc,) was used to more accurately model the 3D nature of the 26th February 2018 slope failure. The ground model was developed based on key geological and geometrical features identified from photogrammetry as previously shown in Figure 3. Ellipsoidal slip surfaces were generated and assessed using various methods of columns calculation algorithms including Bishop, Janbu, Spencer and Morgernstern-Price (GLE). All resulted in similar slip surfaces and factors of safety very close to unity. The ellipsoidal slip surfaces were subsequently altered to find the lowest reasonable factor of safety. The shear strength of the marl at the base of the failed block was determined equal to c'=150kPa and $\varphi=35^0$, while the strength of the back scarp was equal to c'=0kPa and $\varphi=15^0$. The results of the back analysis are shown in Figure 6. The general nature of the slope failure was captured well in three-dimensions with the factor of safety in the model being 1.012 (i.e. close to failure). The 3D modeling approach, effectively identified failure surfaces very similar, from a geometrical perspective, to the actual event on February 26th 2018.

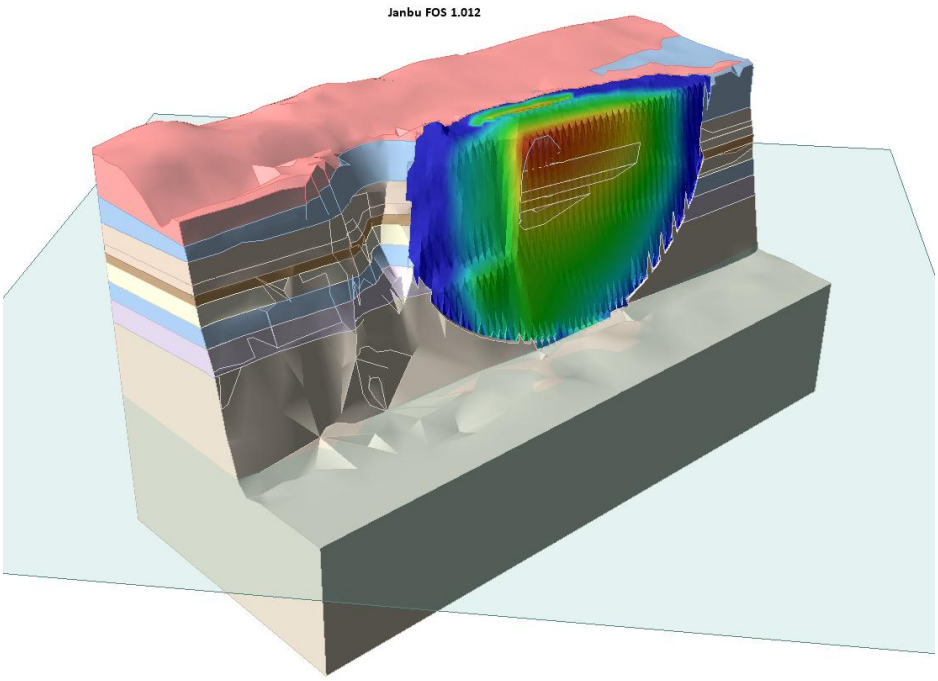

Figure 6. 3D slope stability limit equilibrium analysis results.

CONCLUSIONS

The paper presented the UAV-based mapping and subsequent slope stability analysis of recent failures along the Corinth Canal, highlighting the value of this approach for a relatively quick and accurate assessment of the stability conditions of the cut slopes.

Understanding and being able to realistically model actual ground (geological and geotechnical) conditions is key in developing a robust slope stability model (Bar & Weekes, 2017). The use of 3D models through the Structure-from-Motion technique has facilitated the development of ground models than could otherwise be obtained from boreholes alone. Notwithstanding this, boreholes are essential in understanding conditions behind the exposed slopes and validating the information gathered from the exposures on the slopes.

The failed slope was back-calculated using 2D and 3D limit equilibrium methods and the identified failure surfaces were very similar to the actual event of the February 26th 2018. Concerning the risk of slope failures in the Canal, it is known that the main slides of the Canal have occurred in the past in Zone 3, between

location 1500 and 2000 m while some minor instability problems have occurred in Zone 4, between 2000 and 4600 m. The 2018 failures are located at the south slope at location 2500 m in Zone 4. It is evident that the high risk areas are those where major faults intersect joints forming blocks, which daylight on the slopes and are prone to becoming progressively unstable due to relaxation and strength degradation.

As demonstrated in this paper, the use of new technologies, such as UAV-enabled mapping, in combination with field reconnaissance provides a very effective method for identifying the actual risk areas along the Canal. It also further enables the assessment of slope stability conditions considering different triggering scenarios (rainfall, earthquake etc). The application of such a methodology can also assist in assessing the level of risk due to slope failures along the Canal and allow for preparedness and response strategies in the event of instabilities.

ACKNOWLEDGEMENTS

The authors sincerely thank Dr Andreas Gaich and Dr Markus Pötsch of 3GSM GmbH for the complimentary use of the ShapeMetriX UAV software. In addition, Dr Thamer Yacoub and Ms Alison McQuillan of Rocscience Inc. are also thanked and acknowledged for their continuous support using the latest versions of Slide[3].

REFERENCES

Anagnostopoulos A., Kalteziotis N., Tsiambaos G.K., Kavvadas M. Geotechnical properties of the Corinth Canal marls. *Geotechnical and Geological Engineering* 1991, 9: 1-26.

Andrikopoulou K.P., Marinos P.G., Vainalis D. Geotechnical zoning in the Corinth Canal, *Proc. of an International Symposium on the Engineering Geology of Ancient Works, Monuments and Historical Sites*, 1988; Athens, Greece, Balkema, 1: 231-5.

Bar, N., McQuillan, A. 3D Limit Equilibrium Slope Stability Analysis for Anisotropic and Faulted Rock Masses in Australian Coal and Iron Ore Mines. *Proc. ISRM Int. Symposium 2018, ARMS10*, 2018; Singapore.

Bar, N., Weekes, G. Directional Shear Strength Models in 2D and 3D Limit Equilibrium Analyses to Assess the Stability of Anisotropic Rock Slopes in the Pilbara Region of Western Australia. *Australian Geomechanics Journal* 2017, 52(4): 91-104.

Christoulas, S. G., Kalteziotis, N. A., Tsiambaos, G. K. Geotechnical Problems in a Bridge over Corinth Canal. *International Conference on Case Histories in Geotechnical Engineering*, 1984, 2: 849-854.

CloudCompare (version 2.6) [GPL software], 2015.

Freyberg, V. Geologie des Isthmus von Korinth", Erlangen Geologische Ablhand, Heft 95, 1973: 183 p.

Giordan D., Hayakawa Y., Nex F., Remondino F., Tarolli P. Review article: the use of remotely piloted aircraft systems (RPASs) for natural hazards monitoring and management. *Nat. Hazards Earth Syst. Sci.*, 2018, 18: 1079–1096.

Kallimogiannis V., Saroglou H., Zekkos D., Manousakis J. Back-analysis of landslide in Egremnoi caused by the 2015 Lefkada earthquake. *Proc. of 2nd Int. Conference on Natural Hazards & Infrastructure*, 2019; Chania, Greece.

Kavvadas, M. Some considerations on the stability of the Corinth Canal slopes. *4th Young Geotechnical Engineers Conference*, 1990; Delft, The Netherlands.

Marinos P., Tsiambaos G., Kavvadas M. Geological and geotechnical conditions of the Corinth Canal. *Proc of Engineering Geology and the Environment*, 2001, 3987-4003.

Philippson, A. Der Korinth, Z. Ges. Erdkde. Isthmus von Berlin, 1890: 25, p.1-98

RocPlane. User's Guide, Rocscience Inc, 2002.

Slide[3]. User's Guide, Rocscience Inc, 2019.

Saroglou, C., Asteriou, P., Zekkos, D., Tsiambaos, G., Clark, M., and Manousakis, J.: UAV-based mapping, back analysis and trajectory modeling of a coseismic rockfall in Lefkada island, Greece, *Nat. Hazards Earth Syst. Sci.*, 2018: 18, 321–333.

Zekkos D., Manousakis J., Greenwood W., Lynch J.D., Immediate UAV-enabled Infrastructure Reconnaissance following Recent Natural Disasters: Case Histories from Greece. *Proc. of 1st Int. Conference on Natural Hazards & Infrastructure*, 2016, Chania.

Zekkos, D., Greenwood, W., Manousakis, J., Athanasopoulos-Zekkos, A., Clark, M., Cook, K.L. and Saroglou, C., Lessons Learned from The Application of UAV-Enabled Structure-From-Motion Photogrammetry in Geotechnical Engineering. *International Journal of Geoengineering Case Histories*, 2018: 4 (4), 254-274. doi: 10.4417/IJGCH-04-04-03.

Westoby, M. J., Brasington, J., Glasser, N. F., Hambrey, M. J., and Reynolds, M. J. Structure-from-Motion photogrammetry: A low-cost, effective tool for geoscience applications, *Geomorphology*, 2012: 179, 300–314.